Observation of a two-stage melting transition in two dimensions

Ken Bagchi* and Hans C. Andersen†
Department of Chemistry, Stanford University, Stanford, California 94305

William Swope‡
IBM Almaden Research Center, 650 Harry Road, San Jose, California 95120
(Received 23 October 1995)

We have performed hybrid Monte Carlo and molecular dynamics computer simulations to study the melting transition for a two-dimensional material consisting of classical point particles interacting via an r^{-12} repulsive pair potential. As the density increases, the liquid phase develops hexatic structure at values of the pressure that are too low to allow coexistence with a stable crystal possessing an equilibrium concentration of vacancies. Bond orientational order, translational order, and densities are computed for sub-blocks of the total system. Histograms of these quantities remain unimodal throughout the transition region, indicating no tendency for phase separation. Through the use of block analysis techniques, we extract exponents for the bond orientational and translational correlations in the hexatic and the solid that are consistent with the predictions of the Kosterlitz-Thouless-Halperin-Nelson-Young theory.

I. INTRODUCTION

During the 1970s, Kosterlitz and Thouless [1] advanced a theory for the melting of two-dimensional solids based on the unbinding of dislocation pairs. Young [2] provided additional information about the characteristics of this dislocation-unbinding transition. Halperin and Nelson [3] found that an additional transition, based on the unbinding of disclination pairs, is needed to complete the conversion of a solid to a liquid. The Kosterlitz-Thouless-Halperin-Nelson-Young (KTHNY) theory, as it is commonly called, thus proposes the following two stage scenario for melting: As the temperature of a solid is increased (or the density decreased), the solid undergoes a continuous transition to become a hexatic phase, which is characterized by quasi-long-ranged bond orientational order and finite-ranged translational order. When the temperature is increased (or the density is decreased) further, the hexatic undergoes another continuous transition to become a liquid. This fascinating possibility sparked considerable computer simulation studies, some of which found supporting evidence for this scenario [4–9]. However, a comparable number of studies primarily found evidence for the traditional first-order melting transition [10–15]. It is interesting to note that similar simulation techniques have led to contradictory conclusions, even when applied to the *same material*.

This discrepancy may be a natural result of artifacts that arise in the study of phase transitions using simulations. Near a phase boundary, correlation lengths can be extremely long and thereby introduce spurious results due to finite system size. Similarly, long relaxation times make equilibration difficult and long correlation times make it necessary to do long runs to reduce statistical error. Naidoo, Schnitker, and Weeks [16] confirmed the importance of these problem by studying an r^{-12} potential system; they concluded that the results were sensitive to the choice of boundary conditions and initial configurations. Finite-size scaling analyses, which have been used to circumvent some of these complications, can also be frustrated by the presence of two distinct and long correlations lengths, corresponding to bond orientational and translational order. A review of the KTHNY theory and both experimental and simulation studies can be found in an article by Strandburg [17].

In the present paper, we have applied different equilibration techniques and a block analysis method in a computer simulation study of the r^{-12} potential system. The results show that the traditional first-order melting scenario does not hold for this system. We have found a homogeneous equilibrium phase with hexatic structure and exponents for the bond orientational and translational correlations that agree with the KTHNY theory. In Sec. II we present details of the simulation methods. We follow in Sec. III by giving results for a block analysis used to extract critical exponents for the correlations. Section IV gives details of the pressure data. We finish with conclusions in Sec. V.

TABLE I. Summary of order parameter correlations in various phases.

Correlations	Liquid	Hexatic	Solid
bond orientational	finite correlation length	algebraic decay $0 < \eta_6 < 1/4$	truly long ranged
translational	finite correlation length	finite correlation length	algebraic decay $0 < \eta < 1/3$

*Electronic address: ken@rattle.Stanford.EDU
†Author to whom correspondence should be addressed. Electronic address: fb.hca@forsythe.Stanford.EDU
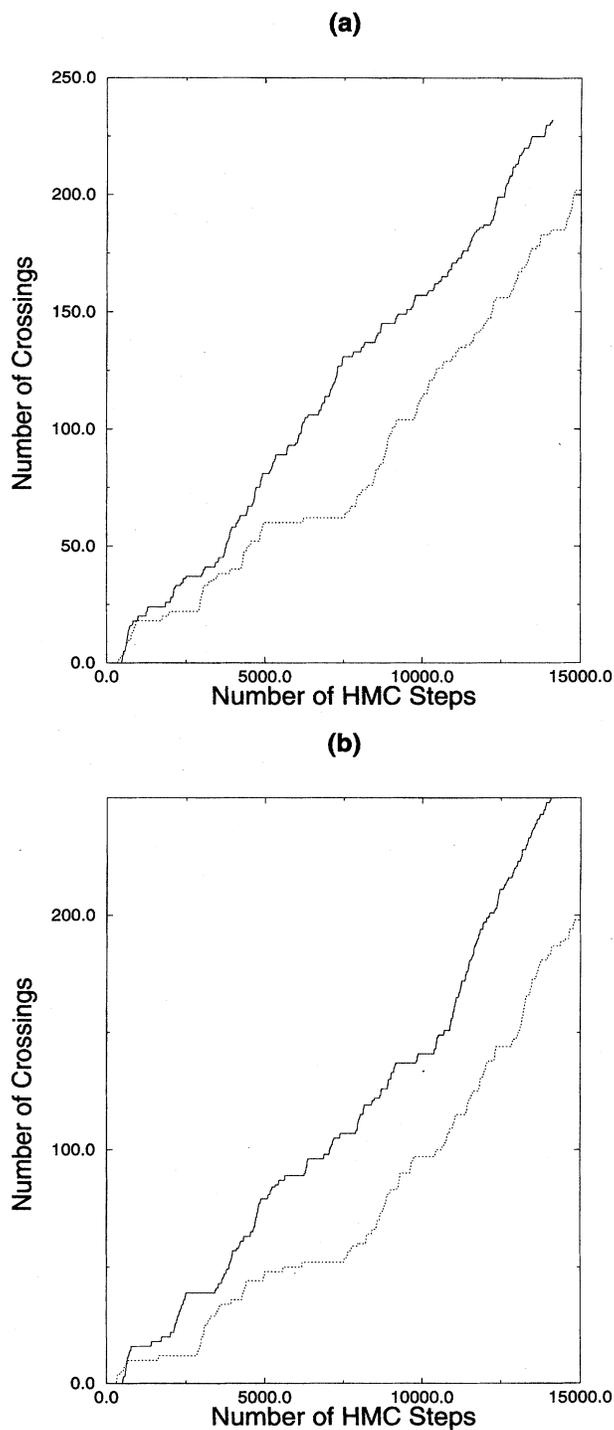‡Electronic address: swope@almaden.ibm.COM

(a)

(b)

FIG. 1. Equilibration and fluctuations with and without the BCE method. (a) The number of times the $\psi^2_{6,c}$ and $\psi^2_{6,r}$ curves cross as a function of the number of HMC steps (see the text for a more complete explanation). (b) A similar plot for ψ^2_t . For both plots, the solid lines correspond to the runs for which the BCE method was used in addition to the HMC method and the dotted lines to runs for which only the HMC method was used.

II. SIMULATION METHODS

The system of interest consists of classical point particles under periodic boundary conditions. The potential of interaction is pairwise additive and of the form $u(r) = \epsilon(\sigma/r)^{12}$, truncated and shifted so that it is continuous and zero for $r \geq 2.5\sigma$ [18]. All data are presented using reduced units such that $\epsilon = 1$, $\sigma = 1$, $m = 1$, and $k = 1$, where k is the Boltzmann constant. Potentials of this form are particularly convenient

TABLE II. MD pressure and chemical potential data for 4096-particle systems. No time-step error corrections have been applied to this data; however, the same time step (0.01τ) was used for all runs. The second column denotes whether the initial configuration was a random liquidlike configuration or a perfect crystal. The third column indicated the length of the run over which the data were collected. The error bars quoted are single standard deviation estimates of the statistical error, computed via a block analysis method [29].

ρ^*	Start	Length (Units of τ)	Pressure (Units of $\epsilon\sigma^{-2}$)	μ (Units of ϵ)
0.9935	random	12 000	14.628 ± 0.006	18.94 ± 0.03
	crystal	12 000	14.617 ± 0.006	19.02 ± 0.04
0.9950	random	24 000	14.670 ± 0.007	19.10 ± 0.02
	crystal	12 000	14.654 ± 0.009	19.01 ± 0.04
1.0000	random	48 000	14.687 ± 0.011	19.08 ± 0.02
	crystal	48 000	14.699 ± 0.009	19.07 ± 0.02

for simulation studies because of a scaling property that allows one to obtain information about transitions along all isotherms from the study of a single isotherm [13,19]. Along the isotherm $T^* = kT/\epsilon = 1$, we simulated the material at various values of the reduced density $\rho^* = (N/V)\sigma^2$, where V is the area of the system. The data presented are for states near $\rho^* = 1$, which previous work has identified as the approximate solid-liquid phase boundary [6,7,13].

To study the effects of finite system size, we did molecular dynamics (MD) simulations with 4096 $(4K)$, 16 384 $(16K)$, and 65 536 $(64K)$ particles under periodic boundary conditions. We employed the velocity Verlet algorithm [20] with a time step of 0.01τ, where $\tau = (m\sigma^2/\epsilon)^{1/2}$, to integrate the equations of motion; stochastic collisions [21] were used to maintain the proper temperature. The pressure was calculated using standard techniques [22].

As can be seen in Table I, the qualitative nature of the bond orientational and translational correlations are distinctively different in liquid, hexatic, and solid phases. Therefore, in addition to estimating the pressure, we calculated both order parameters. The bond orientational order parameter is defined as $\psi_6^2 = |1/6N \sum_l \sum_j \exp(6i\theta_{lj})|^2$, where the sum on l is over all particles, the sum on j is over the nearest neighbors of particle l, and θ_{lj} is the angle between the line joining particle l and particle j and some fixed reference axis. A Voronoi analysis is used to determine which pairs of particles are near neighbors. The translational order parameter can be computed via $\psi_t^2 = |1/N \sum_l \exp(i\mathbf{k} \cdot \mathbf{r}_l)|^2$, where $\mathbf{r}_l$ is the position of particle l. The wave vector $\mathbf{k}$ has a magnitude of $2\pi/\sqrt{\sqrt{3}/2\rho}$, where the denominator is the average lattice spacing. To allow for the possibility of the crystal tilting, we varied the direction of $\mathbf{k}$ over a 120° range; the $\mathbf{k}$ that produced the maximum value of the sum was used to calculate the order parameter.

As we previously mentioned, we were concerned about the ability of standard molecular dynamics to equilibrate states near the transition region. For a solid to form a hexatic, dislocations must form, unbind, and separate. The "climbing" of dislocations, however, essentially amounts to the extension of a row of interstitials or a row of vacancies. This requires the motion of particles over long distances and such motion may be inaccessible on typical MD time scales. Hexatic states may not be seen if solids persist in metastable

phases in the transition region. Similarly, for an isotropic fluid to gain long-range bond orientational order, large numbers of particles must participate in the structural change. Metastable fluids can survive beyond the true limit of liquid stability and eventually freeze into defective solids; this last possibility was in fact seen by Broughton, Gilmer, and Weeks [13].

We have employed a simulation method of Swope and Andersen [23] that was designed to address the problem of equilibrating defects by utilizing the bicanonical ensemble (BCE). This technique has the added benefit of providing the chemical potential for the simulated state. This method involves a particle insertion and deletion process that alternates the total number of particles between N and $N-1$ in accordance with an appropriate detailed balance condition. It can be used with a variety of simulations methods; in the present work, we have used it in conjunction with MD and hybrid Monte Carlo (HMC) methods [24]. The deletion and subsequent insertion of a particle at a different point in the sample greatly enhances not only the net migration of holes and interstitials but also the climb of dislocations as well.

To demonstrate this enhanced equilibration rate, we performed simulations for a 4096-particle system at $\rho^* = 1.004$ starting from two initial states: an almost perfect triangular lattice and a random liquidlike configuration. Using the HMC method, including the BCE insertion and deletion of particles, a simulation was performed using each of these starting states. For each simulation, we computed ψ_6^2 and ψ_t^2 after every ten HMC steps. We denote the results obtained from the run with the crystalline starting state as $\psi_{6,c}^2$ and $\psi_{t,c}^2$ and those from the run with the random initial state as $\psi_{6,r}^2$ and $\psi_{t,r}^2$. Initially, $\psi_{6,c}^2$ and $\psi_{6,r}^2$ are very different because of the qualitative difference in the nature of the initial states. At equilibrium, both $\psi_{6,c}^2$ and $\psi_{6,r}^2$ should fluctuate about the same mean value. We therefore expect that plots of these two data sets versus the number of HMC steps should approach one another as the systems equilibrate and then at equilibrium should cross each other with a mean time between crossings that is related to the correlation time for fluctuations. In Fig. 1 we have plotted the number of times the two curves have crossed as a function of the number of HMC steps that have occurred. We also include a similar plot for ψ_t^2. Then the simulations were repeated, using the same

two initial states, but using only the HMC method with no BCE insertion and deletion. The number of crossings that were observed without BCE insertion and deletion is shown in the figures for comparison. Clearly the BCE simulations have more crossings than simulations with a constant number of particles. Note, especially, that the plateaus in these plots, which are indicative of long-lived fluctuations of the properties of the system, are generally much longer for the simulations with a constant number of particles.

In our "production" MD simulations, we performed two runs at each fluid density studied: one starting from a liquid-like initial configuration and the other from a perfect triangular lattice. Both states were run for 1000τ using only MD and stochastic collisions; no data from this initial equilibration period were considered. The two final configurations were then used as starting states for MD runs that employed the BCE method in addition to stochastic collisions. Data were collected over the next $12\,000\tau$–$48\,000\tau$ and average results are summarized in Tables II and III. At each density, the pressure and chemical potential of the two runs agree within statistical error; given the significantly different initial configurations, this serves as strong proof of the ability of MD simulations of the BCE to equilibrate systems with runs of this duration.

The final configurations from the $64K$ MD runs were then used as starting states for HMC runs. This method has an advantage over MD because it can generate configurations consistent with a canonical distribution without any systematic errors due to nonzero time step. These simulations consisted of $20\,000$–$30\,000$ HMC steps. The duration of the microcanonical runs used to generate the trial configurations was 200 time steps, where the length of a single time step was 0.005τ. This particular combination of parameters produced a 65% acceptance rate.

At equilibrium, the mean value of the chemical potential, pressure, bond orientational order parameter, and translational order parameter should not drift with time. To test for such drift, we use linear regression to fit a line to plots of the various quantities versus the number of HMC steps. For equilibrium systems, the slope of the resulting line must be approximately zero, when statistical error is taken into account. The standard formulas for the slope and its error, however, assume uncorrelated data [25]. We therefore blocked the data until the residuals to the fit were uncorrelated before we applied the standard formulas. Sample plots can be found in Fig. 2. Further details of the analysis are given in the caption of the figure.

III. BOND ORIENTATIONAL AND TRANSLATION ORDER

The nature of the bond orientational and translational order was studied using a block analysis technique, which we applied to the $64K$ particle runs. Each $64K$ configuration was divided into 4 equal sub-blocks (which we refer to as $16K$ sub-blocks since they contain approximately 16 384 particles) and also into 16 equal sub-blocks (which we refer to as $4K$ sub-blocks). Both order parameters were calculated for the entire system and for all the sub-blocks, and average results as a function of (sub-)block size were computed. A plot of the logarithm of an average order parameter versus
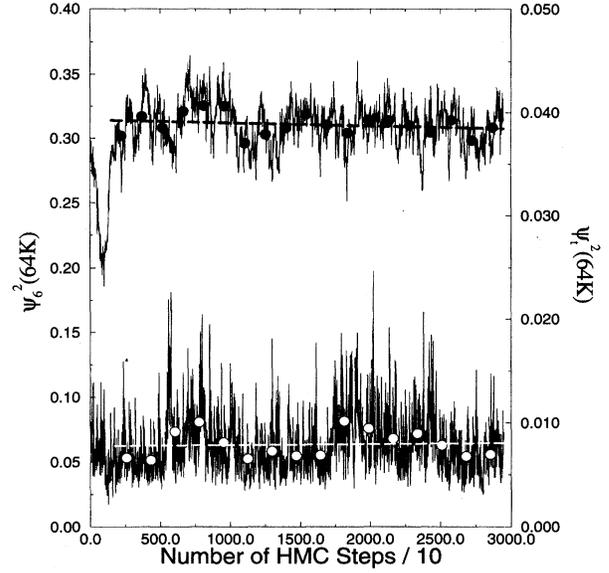

FIG. 2. Time series analysis of ψ_6^2 and ψ_t^2 for $64K$ simulations at $\rho^* = 1.004$. The solid irregular curve represents ψ_6^2 measured after every ten HMC steps. We denote the total number of data points by N. We used linear regression to fit this curve to a line and then computed the residuals. The autocorrelation function of the residuals was calculated and used to determine the number of HMC steps N_c required for this autocorrelation function to decay to zero within the noise. To allow for a possible transient response, the first N_c data points were discarded. The remaining $N' = N - N_c$ points were fit to a line via linear regression; we have shown this fit as a dark dashed line. The autocorrelation function of the residuals from this line were calculated and used to determined N_c', the number of HMC steps required for this autocorrelation function to decay to zero within the noise. The data were grouped into N'/N_c' blocks and averaged within each block. These block averages are shown in dark circles. Since the random errors in these points are uncorrelated, the standard formulas for the slope and its associated error could be then applied [25]. The slope of this line is $-2.3 \times 10^{-6} \pm 2.2 \times 10^{-6}$. Thus this quantity is not drifting with time, when statistical error is taken into account. The data near the bottom and the right axis correspond to a similar plot for ψ_t^2. We have used white circles and white lines for visual reasons. Here the slope was found to $8.1 \times 10^{-8} \pm 4.2 \times 10^{-7}$. Again, this quantity is not drifting with time. Similar analyses were performed on all the $64K$ HMC data to verify the absence of drift. Transients, such as that seen at the far left of the upper curve, are sometimes seen when the final state of a MD calculation is used as the initial state of a HMC calculation. This is related to the fact that the MD results contain systematic error due to nonzero time step, whereas the HMC results represent a true canonical ensemble. The magnitude of the transient appears to be related to the fact that the state being simulated has a very long correlation length, i.e., it is a critical phase with enhanced susceptibility. Similar, but smaller, transients are seen even within MD calculations if the time step is changed. The two stage regression analysis was needed to provide an unbiased way of estimating how much initial data to discard. Only when this data is discarded can we have confidence that the rest of the data can reasonably be fit by a straight line.
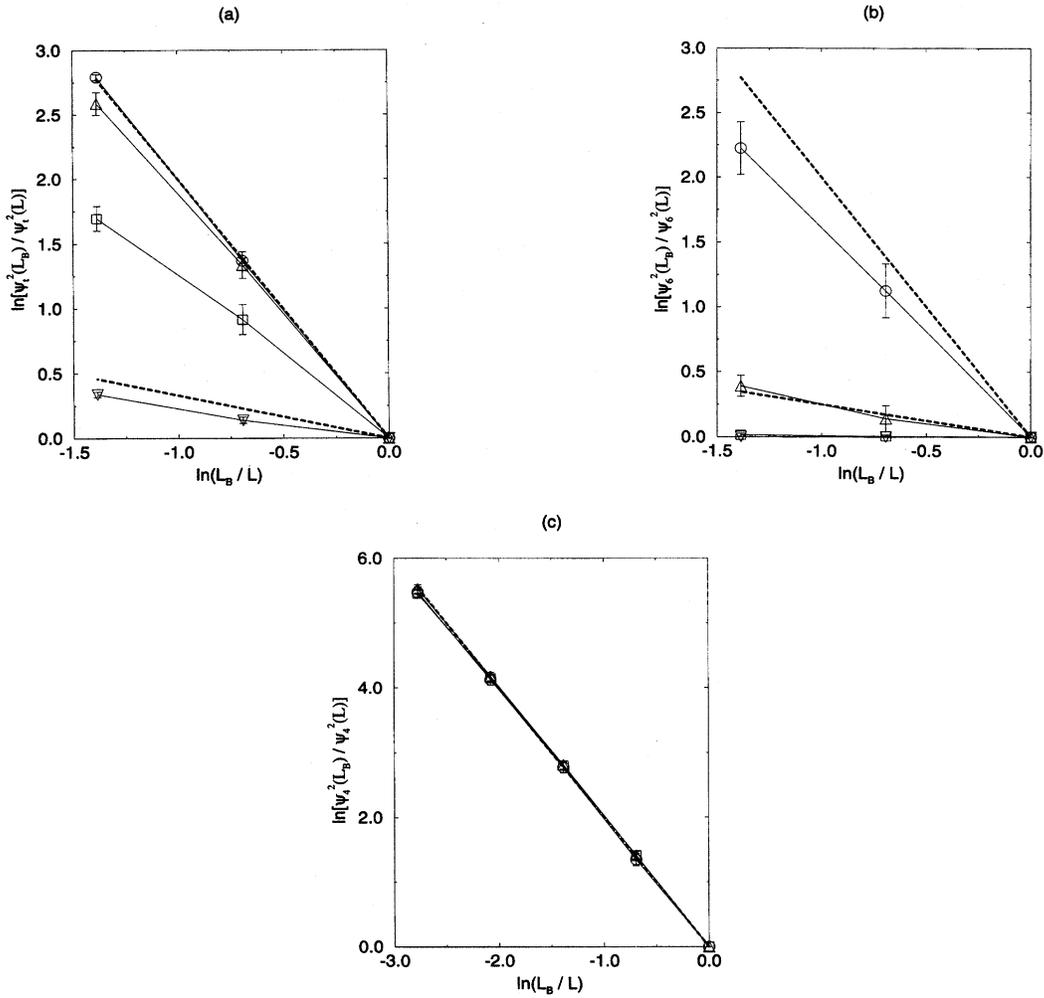
FIG. 3. (a) The natural logarithm of the ratio $\psi_t^2(L_B)/\psi_t^2(L)$ as a function of the natural logarithm of (L_B/L), where $\psi_t^2(L_B)$ is the average translational order parameter for a sub-block of length L_B and L is the length of the total system. Error bars represent single standard deviation error estimates for the ratio. The dark steep dashed line corresponds to a slope of -2, which indicates a finite correlation length. The dark flatter dashed line has a slope of $-1/3$, corresponding to the curve expected at the KT transition. (b) The natural logarithm of the ratio $\psi_6^2(L_B)/\psi_6^2(L)$ as a function of the natural logarithm of (L_B/L), where $\psi_6^2(L_B)$ is the average bond orientational order. Again, the dark steep dashed line has a slope of -2, corresponding to a finite correlation length. The dark flatter line has a slope of $-1/4$, which is the expected power law behavior at the HN transition. (c) The natural logarithm of the ratio $\psi_4^2(L_B)/\psi_4^2(L)$ as a function of the natural logarithm of (L_B/L), where $\psi_4^2(L_B)$ is the average of another bond orientational order parameter discussed in the text. The dark dashed line has a slope of -2, corresponding to a finite correlation length. For all plots, the $\bigcirc$ points correspond to a density of $\rho^* = 0.9935$, the $\triangle$ to a density of $\rho^* = 1.000$, the $\square$ to a density of $\rho^* = 1.007$, and the $\triangledown$ to a density of $\rho^* = 1.0108$. The first three are 65 536-particle systems and the last is a 16 384-particle system.

the logarithm of the (sub-)block length provides a diagnostic about the nature of the correlations.

The basis for this diagnostic is the following analysis. For both order parameters as defined above

$$\psi^2 = \left| \frac{1}{N} \int_V d\mathbf{r}\rho(\mathbf{r}) \right|^2 = \frac{1}{N^2} \int_V d\mathbf{r} \int_V d\mathbf{r}' \rho(\mathbf{r})\rho(\mathbf{r}'),$$

where the integrals are over the area V of the system. In the translational case

$$\rho(\mathbf{r}) = \sum_{i=1}^{N} e^{i\mathbf{k}\cdot\mathbf{r}_i}\delta(\mathbf{r}-\mathbf{r}_i),$$

where $\mathbf{r}_i$ is the position of the ith particle and δ denotes the Dirac delta function. In the bond orientational case

$$\rho(\mathbf{r}) = \frac{1}{6}\sum_{i=1}^{N} \sum_{j}{}' e^{6i\theta_{ij}}\delta(\mathbf{r}-\mathbf{r}_i),$$

where the sum over j is over all near neighbors of particle i. The average order parameter obtained in a simulation,

TABLE III. MD pressure and chemical potential data for 16 384-particle systems. The data are computed and presented in a manner described in Table II.

ρ^*	Start	Length (Units of τ)	Pressure (Units of $\epsilon\sigma^2$)	μ (Units of ϵ)
1.000	random	12 000	14.759 $\pm$ 0.012	19.15 $\pm$ 0.03
	crystal	12 000	14.738 $\pm$ 0.009	19.09 $\pm$ 0.03
1.004	random	12 000	14.717 $\pm$ 0.009	19.11 $\pm$ 0.03
	crystal	12 000	14.711 $\pm$ 0.008	19.06 $\pm$ 0.03
1.007	random	12 000	14.725 $\pm$ 0.013	19.09 $\pm$ 0.03
	crystal	12 000	14.737 $\pm$ 0.010	19.11 $\pm$ 0.03

which we denote $\bar{\psi}^2$, is equivalent to the bicanonical ensemble average of the order parameter. Thus

$$\bar{\psi}^2 = \frac{1}{N^2}\int_V d\mathbf{r}\int_V d\mathbf{r}' \langle \rho(\mathbf{r})\rho(\mathbf{r}')\rangle_V,$$

where $\langle\ \rangle_V$ denotes an ensemble average for an ensemble of area V. The correlation function on the right-hand side is translationally invariant and we define

$$G_V(\mathbf{r}-\mathbf{r}') = \langle \rho(\mathbf{r})\rho(\mathbf{r}')\rangle_V.$$

Making use of the translational invariance, we find

$$\langle \psi^2\rangle_V = \left(\frac{V^2}{N^2}\right)\frac{1}{V}\int_V d\mathbf{r}\, G_V(\mathbf{r}).$$

The factor in large parentheses is an intensive, size-independent quantity.

The simulations can give no information about the correlations for distances larger than the length of the simulation system $L\ (=V^{1/2})$. We assume, however, that

$$G_V(\mathbf{r}) \approx G_\infty(\mathbf{r}) \text{ for } |\mathbf{r}| < L.$$

Hence

$$\bar{\psi}^2 = \left(\frac{V^2}{N^2}\right)\frac{1}{V}\int_V d\mathbf{r}\, G_\infty(\mathbf{r}) \propto \frac{1}{L^2}\int_0^L r\, dr\, G_\infty(\mathbf{r}).$$

We have assumed that the correlation function depends on the scalar distance $r=|\mathbf{r}|$ only. These reasonable assumptions imply that the size dependence of the order parameters is determined by the large-r behavior of the correlation function in the limit of infinite size.

For correlations that decay to zero more rapidly than $1/r^2$, the integral is convergent in the limit of large L and it follows that $\bar{\psi}^2 \propto L^{-2}$ for large L. On the other hand, if

$G_\infty(r) \propto r^{-\eta}$ for large r, with $0 \leq \eta < 2$, then an elementary calculation gives $\bar{\psi}^2 \propto L^{-\eta}[1+O(L^{-2+\eta})]$. Finally, if the correlations are long ranged and $G_\infty(r)$ approaches a nonzero constant for large R, then $\bar{\psi}^2 \propto L^0$ for large L.

The same result is obtained when, instead of considering the entire area of the simulated system, we calculate the order parameter for a part of the system. In this case, replace L by the length of the subsystem studied.

Seeing the predicted asymptotic behavior in simulations of finite size is possible only if a range of values of L can be studied that are all in the asymptotic regime. In the case of finite-ranged correlations, this means having data for a range of L corresponding to distances at which the correlation function is effectively zero. If the data are in the range where the correlation function is small but not zero, $\langle\psi^2\rangle_V$ will decrease *less rapidly* than L^{-2} if the correlation function is positive for large r, which is to be expected for both bond orientational and translational order. In the case of power law decay, the $L^{-\eta}$ behavior will be seen only if L is large enough to make the $L^{-2+\eta}$ correction small. In the case of long-range order, the $O(L^0)$ behavior will be seen only if data are available for values of L large enough that $G_\infty(r)$ has approached its asymptotic value.

To carry out this analysis, we plot $\bar{\psi}^2(L_B)/\bar{\psi}^2(L)$ vs $\ln(L_B/L)$, where L_B is the length of a sub-block of the system and L is the length of the entire system. Figure 3 contains the results for several densities near the phase boundary.

As a test of the method, we computed an order parameter ψ_4^2 that is defined in a way similar to that of ψ_6^2 except that $\exp(6i\theta)$ is replaced by $\exp(4i\theta)$. Because of the predominant sixfold coordination in this material, ψ_4^2 has correlations that are short ranged. The plots in Fig. 3(c) clearly have a slope of -2 at all densities shown, which include states that we shall below identify as liquid, hexatic, and solid.

For a density of 0.9935, Fig. 3(a) indicates that the translational correlations are short ranged. The bond orientational

TABLE IV. $\langle \psi_t^2\rangle$ as a function of sub-block size for different total system sizes at $\rho^*=1.000$. The error bars represent single standard deviation error estimates.

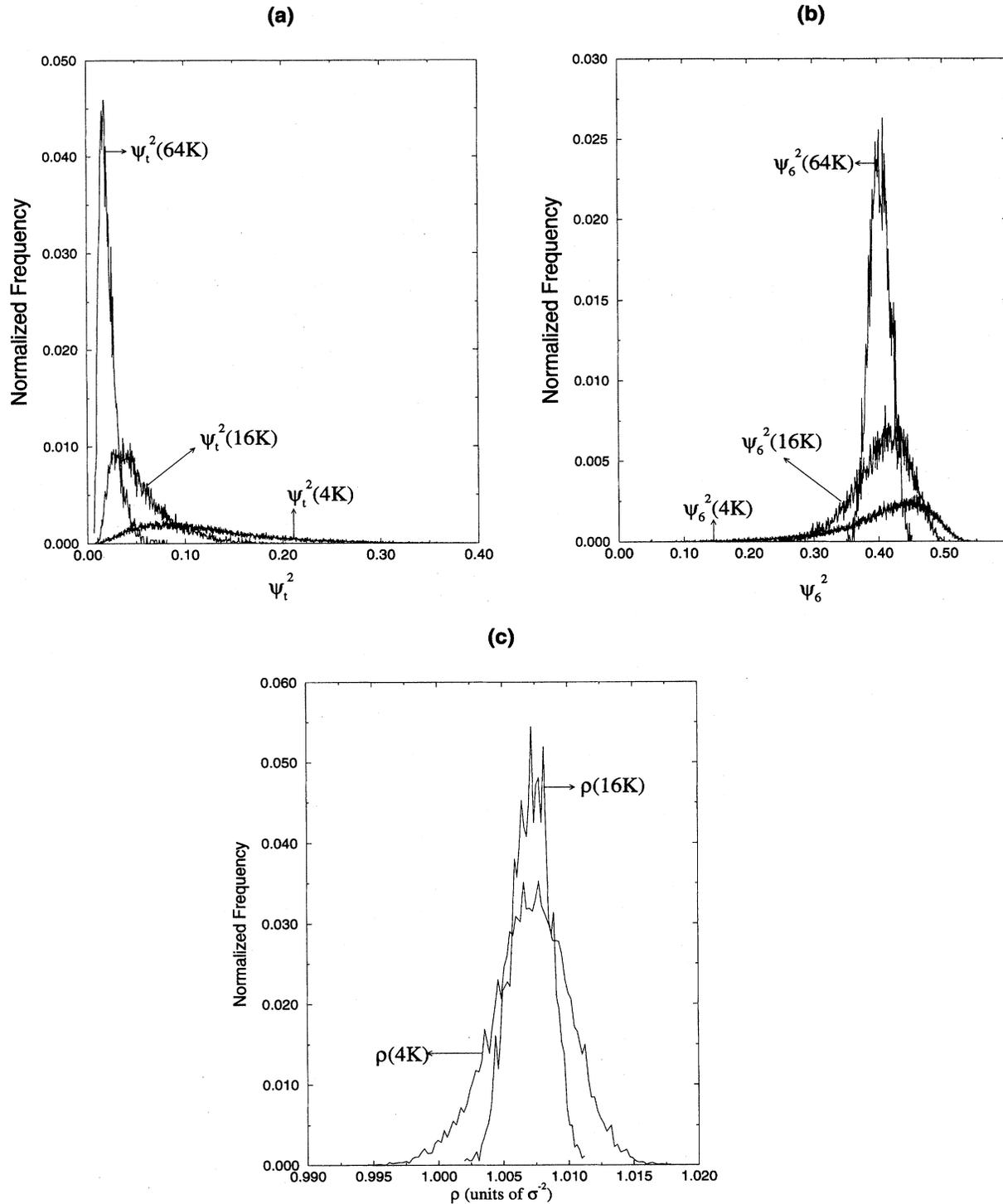| Sub-block size	Total system size 4K	16K	64K
4K	0.051 $\pm$ 0.003	0.036 $\pm$ 0.002	0.033 $\pm$ 0.001
16K		0.012 $\pm$ 0.001	0.0096 $\pm$ 0.0006
64K			0.0025 $\pm$ 0.0002

(a)

(b)

(c)

FIG. 4. (a) Normalized histograms of the translational order parameter for $4K$, $16K$, and $64K$ sub-blocks at $\rho^* = 1.007$. (b) Similar plot for the bond orientational order. (c) Normalized histogram of the density for $4K$ and $16K$ sub-blocks. [The density of the $64K$ system is trivially fixed between N/V and $(N-1)/V$ for a bicanonical simulation.]

order plot for this density in Fig. 3(b) is barely consistent with a slope of -2 and finite range correlations when the slope is calculated using the data for the $16K$ and $64K$ systems. The slope is slightly larger, i.e., less negative, between $4K$ and $64K$, however, suggesting that the correlation length

is of the order of the length of the $4K$ sub-block. The combined behavior leads us to conclude that this state corresponds to a high-density liquid. At $\rho^* = 1.000$, we see that the translational order is still finite ranged, but the translational correlation length has grown to be on the order of the
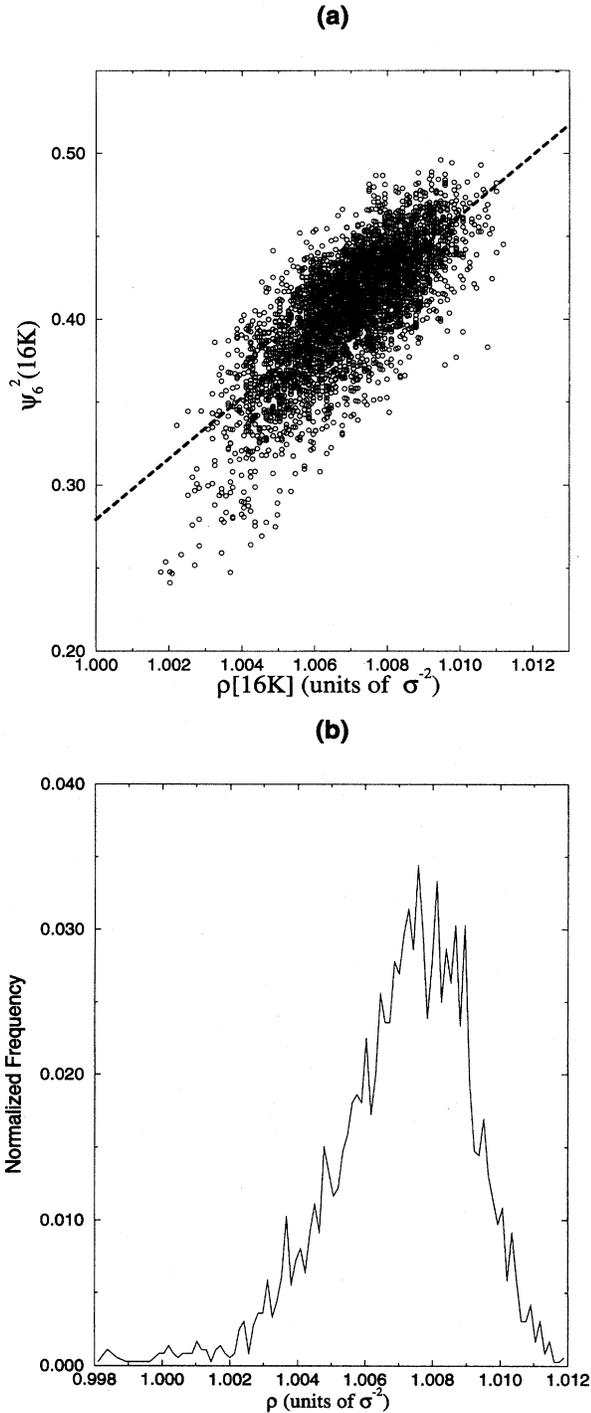
(a)

(b)

FIG. 5. (a) Scatter plot of the bond orientational order parameter versus the density for $16K$ sub-blocks at $\rho^* = 1.007$. The dark dashed line represents a linear regression fit to the data. (b) A histogram of the data after projection on to the linear regression fit.

length of the $4K$ sub-block. The bond orientational curve, in contrast, is now consistent with a power law decay with an exponent of $\eta_6 \sim 1/4$. Hence we identify this state as being at or near the Halperin-Nelson (HN) transition. For
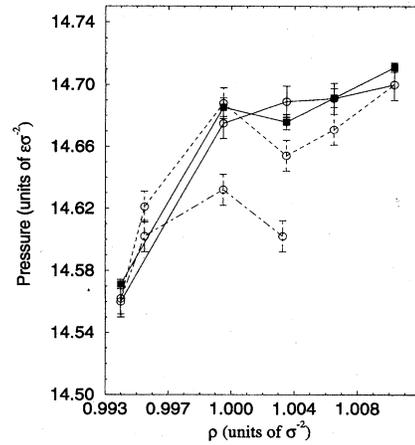

FIG. 6. Pressure as a function of density. The dot-dashed, dashed, and solid lines represent data taken from $4K$, $16K$, and $64K$ simulations, respectively. The filled squares corresponds to HMC data while the open circles represents MD data. Error bars are explained in Table V.

$\rho^* = 1.007$, the translational plot is approximately straight within statistical error, but the slope is too large in magnitude to correspond to a reasonable exponent for translational correlations in a solid (see above). The slight negative curvature suggests that the correlations may be of finite range but with a correlation length that is much larger than the systems studied here. This agrees well with the KTHNY theory, which predicts this correlation length to diverge as it approaches the Kosterlitz-Thouless transition from below. The power law exponent extracted from the bond orientational data for this density is very close to zero, which is again expected for a high-density hexatic. The state with a density of 1.0108 is a solid near the limit of stability of the solid phase [26]. The translational correlations now appear to have a power law decay with an exponent less than 1/3. Within noise, the power law exponent for the bond orientational correlations is zero; this is consistent with the prediction of true long-range order in the solid.

Above we concluded that the state at a reduced density of 1.000 was at or near the HN transition. The curvature of the translational order parameter plots suggests that the translational correlation length at this density is of the order of the length of a $4K$ sub-block. If this were the case, we might expect that periodic boundary condition simulations of a $4K$ system might tend to stabilize the crystalline order and lead to a larger average order parameter than would be seen in a $4K$ sub-block of a larger system simulated using periodic boundary conditions. To test this suggestion, we performed HMC simulations at this density using periodic boundary conditions for system containing $4K$, $16K$, and $64K$ particles. We computed the average translational order parameter for the $4K$ periodic system and for $4K$ sub-blocks of the $16K$ and $64K$ periodic systems; we have summarized the results in Table IV. The values obtained for the $4K$ sub-blocks of the larger systems agreed, within statistical error. The value for smallest system, however, was clearly much larger. In contrast, the average value for the $16K$ periodic system and for the $16K$ sub-blocks of the $64K$ periodic sys-

TABLE V. Pressure data. The first column lists the reduced densities. The remaining columns give the pressure data in reduced units of $\epsilon\sigma^2$. The MD data have been corrected for the effect of nonzero time step. The error bars for the MD data are estimates of the error in this correction. The error bars for the HMC data represent single standard deviation estimates of the statistical error.

| | Pressure | | | |
| | MD | | | HMC |
ρ^*	4096 particles	16 384 particles	65 536 particles	65 536 particles
0.9935	14.562 ± 0.01	14.562 ± 0.01	14.560 ± 0.01	14.571 ± 0.003
0.9950	14.602 ± 0.01	14.621 ± 0.01		
1.0000	14.632 ± 0.01	14.688 ± 0.01	14.675 ± 0.01	14.685 ± 0.006
1.003 77	14.602 ± 0.01			
1.0040		14.654 ± 0.01	14.689 ± 0.01	14.676 ± 0.005
1.0070		14.671 ± 0.01	14.691 ± 0.01	14.691 ± 0.006
1.0108		14.700 ± 0.01	14.700 ± 0.01	14.711 ± 0.003

tem almost agreed, when statistical error was taken into account. This confirms the suggestion that at this density the translational correlation length is finite and on the order of the length of the $4K$ cell.

A long, but finite, translational correlation length at hexatic densities could complicate certain finite-size scaling analyses. A histogram method by Lee and Kosterlitz [27] and a fourth-order cumulant method by Binder [28] can be appropriately applied only at system sizes that are "sufficiently large so that irrelevant fields have been scaled away" [14]. This means that, for hexatic states, the length of sub-blocks studied must be larger than the finite translational correlation length. Lee and Strandburg [14] and Weber and Marx [15] have applied such finite-size scaling techniques to the study of hard disk melting; they concluded that a traditional first-order melting transition occurs at $\rho^* \sim 0.9$. The largest system studied by Lee and Strandburg was only 400 particles. The total system sizes studied by Weber and Marx are quite large; however, the largest sub-block analyzed contained only 1024 particles. Given the similarities between the hard disk potential and the r^{-12} potential, it seems plausible that such sub-block lengths are not large compared to the finite translational correlation length near the melting transition. If this is in fact the case, a more complicated analysis may be required before any conclusions can be drawn about the nature of the transition.

In addition to calculating the average of both order parameters for various sub-block sizes, we also computed histograms of the distribution of values of the order parameters and of the density. If the system separates into distinct phases, histograms of all three quantities should show a bimodal distribution. The two peaks would then correspond to the values for the coexisting phases. Alternatively, if the systems are homogeneous, as expected for continuous transitions, these plots should be unimodal. In Fig. 4 we have plotted some representative histograms for $\rho^* = 1.007$. Clearly, all the graphs are unimodal. These are typical of the distributions found at all densities studied. It may also be informative to examine the joint distribution of two or more of these quantities. The existence of two "islands" in a scatter plot of these quantities would be a sign of two-phase coexistence, while a single island would denote a homogeneous material. Figure 5 shows such a plot and again confirms the homogeneous nature of our system. In summation, the data presented in this section identify a range of reduced densities from 1.000 to 1.007 with hexatic correlations and provide strong support that such states are homogeneous with no tendency for phase separation.

IV. PRESSURE DATA

We have summarized the pressure data as a function of density in Fig. 6 and Table V. Raw pressure data obtained from MD simulations contain systematic errors due to nonzero time step. For sufficiently small time steps, this error should grow quadratically with time step, under velocity Verlet integration. We performed short MD runs and plotted the mean pressure as a function of the square of the time step [23]. By linearly extrapolating to zero time step, we estimated the magnitude of the systematic error. For a time step of 0.01τ, we found this error to be 0.06 ± 0.01 in the transition region. We have applied this correction to the MD pressure data reported in this section. The statistical errors are not quoted since they are smaller than the error in the time-step correction. The HMC data, in contrast, contains no systematic error due to nonzero time step and the uncertainties reported are the relatively small statistical errors.

As we will discuss in detail elsewhere [26], the state with a density of 1.0108 is very near the lower limit of stability of the solid with an equilibrium concentration of vacancies. According to the more accurate HMC data, the pressure of this state is higher than those of the liquid and hexatic states with a reduced density of 1.007 and less. Therefore, the transition out of the solid cannot be of the traditional first-order type to a liquid with short-ranged bond orientational order. We were unable to equilibrate states within a density of about $0.1-0.2$ % of the lower limit of solid stability and hence we cannot comment directly on the nature of the transition from the solid to the hexatic.

At this point, we concentrate on data for the liquid and hexatic states with $\rho^* \leq 1.007$. For the $4K$ and $16K$ MD simulations, the pressure data as a function of density show a maximum, which might be interpreted as a van der Waals loop. Such a feature is normally taken as evidence for a first-order transition. As the system size increases, however, the amplitude of the oscillation and the apparent width de-

creases. At the $64K$ size, the MD data are monotonically increasing throughout the transition region. The $64K$ HMC data are consistent with both the MD data and a monotonic rise, when statistical error is taken into account. The trend of the pressure data with system size leads us to conclude that there is no first-order transition in the thermodynamic limit in this density range. Given the uncertainties, however, we cannot rule out a narrow first-order transition with coexisting densities separated by less than 0.5%; if such a transition were to exist, it would be in a range of densities for which only liquid and hexatic states are stable.

V. CONCLUSION

The thermodynamic data presented in the paper clearly rule out a first-order phase transition from a liquid with short-ranged bond orientational order to a solid with an equilibrium concentration of vacancies. Density and order parameter histograms show that the intervening phase is homo-geneous; block analysis gives critical exponents for the bond orientational and translational correlations for the intervening phase that are in agreement with the KTHNY predictions for a hexatic. A simple and consistent interpretation of the data is that the r^{-12} pair potential in two dimensions has a Halperin-Nelson second-order transition and a Kosterlitz-Thouless second-order transition, with an intervening hexatic phase that is stable over a range of densities that is about 1.2% wide. The pressure-density isotherm is very flat at the hexatic densities and we cannot rule out a first-order transition. In such a case, however, it must lie in a density range for which only liquid and hexatic states are stable.

[1] J.M. Kosterlitz and D.J. Thouless, J. Phys. Chem. **6**, 1181 (1973).

[2] A.P. Young, Phys. Rev. B **19**, 1855 (1979).

[3] B.I. Halperin and D.R. Nelson, Phys. Rev. Lett. **41**, 121 (1978); D.R. Nelson and B.I. Halperin, Phys. Rev. B **19**, 2457 (1979).

[4] D. Frenkel and J.P. McTague, Phys. Rev. Lett. **42**, 1632 (1979).

[5] J. Tobochnik and G.V. Chester, in *Ordering in Two Dimensions*, edited by S.K. Sinha (North-Holland, Amsterdam, 1980), p. 339.

[6] J.A. Zollweg, G.V. Chester, and P.W. Leung, Phys. Rev. B **39**, 9518 (1989).

[7] J.A. Zollweg and G.V. Chester, Phys. Rev. B **46**, 11 186 (1992).

[8] K. Naidoo and J. Schnitker, J. Chem. Phys. **100**, 3114 (1994).

[9] K. Chen, T. Kaplan, and M. Mostoller, Phys. Rev. Lett. **74**, 4019 (1995).

[10] F.F. Abraham, Phys. Rev. Lett. **44**, 463 (1980); F.F. Abraham, in *Ordering in Two Dimensions* (Ref. [5], p. 155; J.A. Barker, D. Hendersen, and F.F. Abraham, Physica A (Utrecht) **106**, 226 (1981).

[11] S. Toxvaerd, Phys. Rev. Lett. **44**, 1002 (1980).

[12] F. van Swol, L.V. Woodcock, and J.N. Cape, J. Chem. Phys. **73**, 913 (1980).

[13] J.Q. Broughton, G.H. Gilmer, and J.D. Weeks, Phys. Rev. B **25**, 4651 (1982).

[14] J. Lee and K. Strandburg, Phys. Rev. B **46**, 11 190 (1992).

[15] H. Weber and D. Marx, Europhys. Lett. **27**, 593 (1994).

[16] K. Naidoo, J. Schnitker, and J.D. Weeks, Mol. Phys. **80**, 1 (1993).

[17] K.J. Strandburg, Rev. Mod. Phys. **60**, 161 (1988).

[18] That is, the potential actually used in the simulations was $u(r) = \epsilon(\sigma/r)^{12} - \epsilon(\sigma/r_c)^{12}$ for $r \le r_c$ and $u(r) = 0$ for $r \ge r_c$, where $r_c = 2.5\sigma$. The truncation and shifting causes only a minor change in the potential; at $r = r_c$ the untruncated potential has a value of $1.7 \times 10^{-5} \epsilon$. The second virial coefficient of the truncated and shifted potential is $1.772\,926\sigma^2$, very close to that of the untruncated potential, namely $1.773\,095\sigma^2$.

[19] Strictly speaking, the scaling property applies only to the untruncated potential.

[20] W.C. Swope, H.C. Andersen, P.H. Berens, and K.R. Wilson, J. Chem. Phys. **76**, 637 (1982).

[21] H.C. Andersen, J. Chem. Phys. **72**, 2384 (1980).

[22] M.P. Allen and D.J. Tildesley, *Computer Simulation of Liquids* (Clarendon, Oxford, 1987), p. 47.

[23] W.C. Swope and H.C. Andersen, J. Chem. Phys. **102**, 2851 (1995).

[24] S. Duane, A.D. Kennedy, B.J. Pendelton, and D. Roweth, Phys. Rev. Lett. **195**, 216 (1987); S. Gupta, A. Irbäck, F. Karsh, and B. Petersson, Phys. Lett. B **242**, 437 (1990); R. Gupta, G.W. Kilcup, and S.R. Sharpe, Phys. Rev. D **38**, 1278 (1988); A.D. Kennedy and B. Pendleton, Nucl. Phys. B (Proc. Suppl.) **20**, 118 (1991); M.E. Clamp, P.G. Baker, C.J. Stirling, and A. Brass, J. Comput. Chem. **15**, 838 (1994).

[25] P.J. Diggle, *Time Series* (Oxford University Press, Oxford, 1990); J.D. Cryer, *Time Series Analysis* (PWS-Kent, Boston, 1986).

[26] H.C. Andersen, K. Bagchi, and W.C. Swope (unpublished).

[27] J. Lee and J.M. Kosterlitz, Phys. Rev. Lett. **65**, 137 (1990); Phys. Rev. B **43**, 1268 (1991).

[28] K. Binder, Phys. Rev. Lett. **47**, 693 (1981); Z. Phys. B **43**, 119 (1981).

[29] H. Flyvbjerg and H.G. Petersen, J. Chem. Phys. **91**, 461 (1989).